Extended three-cluster model with two-cluster long-range correlations: Application to the ^{8}Li, ^{8}B nuclei

L. V. Grigorenko,[1,2,3,*] B. V. Danilin,[1,2] V. D. Efros,[1,2] N. B. Shul'gina,[2,3] and M. V. Zhukov[3]
[1]*Physics Department, University of Surrey, Guildford, Surrey GU2 5XH, United Kingdom*
[2]*Russian Research Center ''The Kurchatov Institute,'' RU-123182 Moscow, Russia*
[3]*Department of Physics, Chalmers University of Technology, S-41296 Göteborg, Sweden*
and Department of Physics, Göteborg University, S-41296 Göteborg, Sweden
(Received 23 March 1999; published 9 September 1999)

A technique for the direct treatment of asymptotic binary channels in three-body systems with bound subsystems is developed in the framework of the hyperspherical harmonic (HH) method. The method is tested on the well-studied ^{6}Li nucleus. Comparison with ''pure'' HH calculations shows faster convergence of the binding energy and larger matter radii. The model problem ''^{6}Li'' with a very loosely bound deuteron is considered and the result demonstrates the efficiency of the method in this case. The low-lying three-cluster states in ^{8}Li and ^{8}B spectra are studied; various observables for such states are calculated in a three-body $\alpha + {}^3\mathrm{H}({}^3\mathrm{He}) + N$ model. [S0556-2813(99)01010-9]

PACS number(s): 21.60.Gx, 21.45.+v, 27.20.+n

I. INTRODUCTION

In this paper we develop simple techniques for the treatment of long-range two-cluster correlations in the framework of a three-cluster model, and we apply this approach to study the structure of ^{8}Li and ^{8}B nuclei. While the issue of the applicability of three-cluster models is of interest itself, the structure of these nuclei is of importance for nucleosynthesis and boron solar neutrino problems as well. Despite intensive studies, both experimental and theoretical, many features of the structure of these nuclei are not well established yet.

Three-cluster descriptions of the ^{8}Li and ^{8}B nuclei [1,2] seem to be very natural and transparent. In the framework of such descriptions the effects of the distortion of the two-cluster cores ^{7}Li and ^{7}Be are taken into account, and this goes beyond the binary potential models ([3], and references therein). Alternative clusterizations having higher separation energies are disregarded within the simple three-cluster model we use. Those clusterizations would reduce two- and three-cluster spectroscopic factors for decays into the main cluster configurations. Nevertheless, one can expect that such effects are merely small corrections.

Two extreme situations may take place in a three-cluster system. In one of them the removal energy of a cluster is much lower than the binding energy of the residual two-cluster subsystem. In such a case two-body models can take account of many properties of a system and corresponding long-range two-body correlations. Another extreme occurs when there are no bound states in any of two-body subsystems (so-called ''Borromean'' situation; see the reviews in [4–6] and references therein). Strong long-range two-cluster correlations are absent in this case. The hyperspherical expansion of the wave function (WF) is convenient to describe such systems [7,4]. The hyperspherical harmonic (HH) approach has also been used for many years in the three-nucleon problem and is known to ensure highly accurate results for the ''democratic'' ^{3}H and ^{3}He systems [8]. Indeed, for Borromean systems, only the few lowest order terms in the expansion contribute significantly to most of the physical observables (provided that binary interactions do not contain strong repulsive cores). This is especially true when the binding energy is small and the three-cluster asymptotics of the WF contributes predominantly to the observables. However, in the general case of loosely bound systems both two-body and three-body asymptotics of the WF are significant, and this applies to the ^{8}Li and ^{8}B nuclei. One may still use the HH expansion to describe such systems but the expansion of the outer two-body part of the WF over the HH basis may converge very slowly.

Since use of the HH expansion has many advantages in the three-body breakup region, it would be desirable to utilize it despite the above difficulty. However, the method needs to be modified to cope with the two-body long-range asymptotics. In fact, it has been known for many years how to avoid the problems mentioned above [9–11]. The idea is connected with the fact that the form of the two-body outer components of the WF (both for open and closed channels) is well known,[1] and these components can be written down in an explicit form. If we subtract these components with unknown coefficients from the WF, then the remainder will have mainly the three-body asymptotics, and it can be readily expanded over the HH basis. This method was called the *interpolation approach* (IA). It has been used a few times [11,12] and has shown its applicability.[2] The procedure enables us to avoid matching the interior WF with the asymptotic binary WF, which is not a well-defined procedure for a few-body WF. Physically the approach is close to

*Electronic address: L.Grigorenko@surrey.ac.uk

[1]In this paper we consider only the case of closed two-body channels.

[2]The lack of powerful computers at that time inhibited wider applications.

Feshbach's method [13] and also to the inclusion of distortion terms in the framework of the resonating group method (RGM) [14].

The main difficulty with such an approach is the necessity to compute rather complicated nonstandard matrix elements which are given by five-dimensional integrals. Here the method loses one of the advantages of the standard HH approach.

In this paper we apply the IA to study the three-cluster nuclei. In Sec. II we demonstrate that it is possible to avoid computations of the complicated matrix elements and deal only with the simple HH matrix elements. In Sec. III it is shown that in the case of the ^{6}Li nucleus the inclusion of the two-body, or binary channel (BC), components into the WF yields much faster energy convergence and leads to a larger matter radius as compared with the ordinary HH calculations. In Sec. IV the approach is tested for the model case of a three-cluster system extremely weakly bound with respect to the two-body decay. While the ordinary HH expansion runs into problems in this case, the new method remains applicable. The real example of such a system is the ^{8}B nucleus which is bound by only 0.138 MeV relative to the two-body $^7\mathrm{Be}+p$ threshold and by 1.725 MeV relative to the three-body $\alpha+{}^3\mathrm{He}+p$ threshold. Study of the structure of the ^{8}Li and ^{8}B nuclei is presented in Sec. V.

We use units $\hbar=c=1$. The notation ''t'' stands for the ^{3}H cluster in ^{8}Li and the ^{3}He cluster in ^{8}B.

II. THREE-BODY BOUND STATE WITH BINARY CHANNEL

Working with a three-body system it is convenient to introduce translationally invariant normalized sets of Jacobi coordinates $\mathbf{x}$, $\mathbf{y}$:

$$\mathbf{x}_3=C_x\mathbf{X}_3=C_x(\mathbf{R}_1-\mathbf{R}_2),\quad C_x=\sqrt{\frac{A_1A_2}{A_1+A_2}},\tag{1}$$

$$\mathbf{y}_3=C_y\mathbf{Y}_3=C_y\left(\frac{A_1\mathbf{R}_1+A_2\mathbf{R}_2}{A_1+A_2}-\mathbf{R}_3\right),$$

$$C_y=\sqrt{\frac{(A_1+A_2)A_3}{A_1+A_2+A_3}}.\tag{2}$$

Where A_i and $\mathbf{R}_i$ is the mass number and the coordinate of the ith particle. Assuming that the third particle is an α particle for ^{6}Li and a neutron (proton) for ^{8}Li (^{8}B), the ''physical'' Jacobi coordinates $\mathbf{X}_3=\mathbf{R}_{12}$ and $\mathbf{Y}_3=\mathbf{R}_{(12)3}$ are scaled:

$$A=6,\quad \mathbf{x}_3=\sqrt{1/2}\mathbf{R}_{12},\quad \mathbf{y}_3=\sqrt{4/3}\mathbf{R}_{(12)3},$$

$$A=8,\quad \mathbf{x}_3=\sqrt{12/7}\mathbf{R}_{12},\quad \mathbf{y}_3=\sqrt{7/8}\mathbf{R}_{(12)3}.$$

Alternative sets of Jacobi coordinates are obtained by cyclic permutations of (1,2,3). Below we shall use hyperspherical coordinates ρ and θ,

$$\rho^2=(x^2+y^2)=\frac{1}{A_1+A_2+A_3}\sum_{i,j=1,i>j}^{3}A_iA_j(\mathbf{R}_i-\mathbf{R}_j)^2,$$

$$\theta=\arctan(x/y),\quad x=\rho\sin(\theta),\quad y=\rho\cos(\theta).$$

Here the hyperradius ρ is a collective rotationally and permutationally invariant variable.

In the three-body representation of $A=6$ and $A=8$ nuclei (for details see [4,1]), the cluster-cluster interactions depend only on intercluster distances and cluster spins and isospins. After separation of the c.m. motion the ''active'' WFs have the form

$$\Psi^T_{JM}(\mathbf{X},\mathbf{Y},\sigma_{zi},\tau_{zi}),\tag{3}$$

where σ_{zi} and τ_{zi} are cluster spin and isospin variables. J, M, and T are, respectively, the total angular momentum, its projection, and total isospin. The WFs (3) are the object of three-body calculations. Clusters are completely inert in this approach, and in order to obtain complete microscopic WFs from Eq. (3) one should replace cluster spin and isospin functions entering Eq. (3) by intrinsic cluster WFs with given spin and isospin projections. In the present work the effects of antisymmetrization with respect to nucleons belonging to different clusters were taken into account approximately in the usual way by employing repulsive intercluster interactions in s waves. There exists an alternative approximate procedure, namely, use of intercluster potentials with forbidden states and reduction of the space of three-body states via projecting out the two-cluster forbidden states. The two procedures were compared with each other in a number of papers [15,4,16], and practically no differences in values of the observables of the types we consider were found.

A disadvantage of the HH method, in the case when a bound two-body subsystem is present, is that it does not provide the true asymptotic behavior of the WF at large ρ. Formally, the HH basis is complete on the hypersphere of fixed hyperradius. So at a given ρ value one can reproduce the WF with any precision, increasing the number of basis HHs. However, for some physical problems, requiring exact knowledge of the asymptotics, the computational power may expire faster than the necessary precision is achieved. We are going to resolve this problem, writing Ψ^T_{JM} as a sum of the ''democratic'' three-body function $\Psi^{(3)T}_{JM}$ and the cluster $\alpha+d$ function $\Psi^{(2)T}_{JM}$ for ^{6}Li (or $^7\mathrm{Li}+n$, $^7\mathrm{Be}+p$ function for ^{8}Li, ^{8}B), thus ''forcing'' Ψ^T_{JM} to have the correct binary asymptotics:

$$\Psi^T_{JM}=\Psi^{(3)T}_{JM}+\Psi^{(2)T}_{JM,\mathrm{ort}}.\tag{4}$$

Here $\Psi^{(3)T}_{JM}$ is a standard HH method WF in LS coupling,

$$\Psi^{(3)T}_{JM}=\rho^{-5/2}\sum_{K=K^{(3)}_{\min},\gamma}^{K^{(3)}_{\max}}\chi_{K,\gamma}(\rho)\mathcal{J}_{K,\gamma}(\Omega_5)\chi_{TM_T}. \quad (5)$$

In Eq. (5), K is the generalized angular momentum quantum number, and the multiindex γ denotes collectively the orbital momentum and spin quantum numbers,

$$\gamma=\{L,l_x,l_y,S,S_x\}.$$

The notation $\Omega_5=\{\theta,\hat{n}_x,\hat{n}_y\}$ is used in Eq. (5), and $\mathcal{J}_{K,\gamma}$ are basis HHs having the explicit form

$$\mathcal{J}_{K,\gamma}(\Omega_5)=\psi^{l_xl_y}_K(\theta)[[Y_{l_x}(\Omega_x)\otimes Y_{l_y}(\Omega_y)]_L\otimes\chi_S]_{JM},$$

$$\chi_{SM_s}=[[\chi_{S_1}\otimes\chi_{S_2}]_{S_x}\otimes\chi_{S_3}]_{SM_s},$$

where χ_S includes spins of nucleons or constituent clusters. The hyperangular eigenfunctions $\psi^{l_xl_y}_K$ are proportional to Jacobi polynomials $P^{\alpha,\beta}_n$,

$$\psi^{l_xl_y}_K(\theta)=N^{l_xl_y}_K(\sin\theta)^{l_x}(\cos\theta)^{l_y}P^{l_x+1/2,l_y+1/2}_{(K-l_x-l_y)/2}(\cos 2\theta). \quad (6)$$

The expansion (5) is truncated at $K=K^{(3)}_{\max}$, and in accordance with Eq. (6), the value $K^{(3)}_{\min}=l_x(\min)+l_y(\min)$ is determined by the lowest l_x and l_y in the expansion.

The WF (5) has a standard three-body bound state asymptotics, which is (without Coulomb interaction)

$$\Psi^{(3)T}_{JM}\overset{\rho\to\infty}{\sim}\rho^{-5/2}\exp\{-\kappa\rho\}, \quad (7)$$

$$\kappa=\sqrt{k_x^2+k_y^2}=\sqrt{2M(E_x+E_y)}=\sqrt{2ME_{3\text{sep}}},$$

where M is the nucleon mass,[3] $E_{3\text{sep}}$ is the binding energy of the system relative to the three-body breakup threshold, and $\mathbf{k}_x$ and $\mathbf{k}_y$ are normalized Jacobi momenta conjugated to $\mathbf{x}$ and $\mathbf{y}$.

$\Psi^{(2)T}_{JM}$ in Eq. (4) is a two-body cluster WF in a physically motivated jj representation, $j_x=l_x+S_x$, $j_y=l_y+S_3$:

$$\Psi^{(2)T}_{JM}=\sum_i f_i(\rho)\mathcal{B}_i(\mathbf{X},\mathbf{Y})\chi_{TM_T}. \quad (8)$$

The different binary channels are numerated by the set of quantum numbers (multi-index) i:

$$i=\{l_x,j_x,l_y,j_y\},$$

$$\mathcal{B}_i(\mathbf{X},\mathbf{Y})=[\psi_{l_xj_x}(\mathbf{X})\otimes\psi_{l_yj_y}(\mathbf{Y})]_{JM}. \quad (9)$$

It is convenient to represent the quantity (9) in the LS coupling form

$$\mathcal{B}_i(\mathbf{X},\mathbf{Y})=\sum_{LS}\frac{\psi_{l_xj_x}(X)\psi_{l_y}(Y)}{XY}\hat{L}\hat{S}\hat{j}_x\hat{j}_y\begin{Bmatrix}l_x & S_x & j_x\\ l_y & S_3 & j_y\\ L & S & J\end{Bmatrix}\times[[Y_{l_x}(\Omega_x)\otimes Y_{l_y}(\Omega_y)]_L\otimes\chi_S]_{JM}. \quad (10)$$

Here $\psi_{l_xj_x}(X)$ are the radial components of the binary subsystem WF with angular and total momenta l_x and j_x. They are obtained using the same potential as used for the three-body calculations, and their asymptotics are

$$\psi_{l_x}(X)\overset{X\to\infty}{\sim}W_{-\eta_x,l_x+1/2}(2K_xX),$$

$$K_x=\sqrt{2M_xE_x},\quad \eta_x=\frac{Z_1Z_2\alpha}{v_x}=Z_1Z_2\alpha\sqrt{\frac{M_x}{2E_x}}, \quad (11)$$

where M_x and E_x are the reduced mass and binding energy of the binary subsystem. The function $\psi_{l_y}(Y)$ is the binary relative motion WF (subsystem $1+2$ with respect to particle 3) with definite angular momentum l_y. The function $\psi_{l_y}(Y)$ is taken independent of j_y. Outside the interaction region $\psi_{l_y}(Y)$ turns to the (Coulomb) Whittaker function determined by the cluster separation energy E_y. Its asymptotics for large Y is

$$\psi_{l_y}(Y)\overset{Y\to\infty}{\sim}W_{-\eta_y,l_y+1/2}(2K_yY), \quad (12)$$

$$K_y=\sqrt{2M_y|E_y|}=\sqrt{2M_y|E_{3\text{sep}}-E_x|}. \quad (13)$$

Inside the interaction region this function is rather arbitrary. We obtained $\psi_{l_y}(Y)$ as a bound state in a Gaussian potential (plus a proper Coulomb, if any). The depth of the potential was varied to get the correct separation energy. The width $a_{(12)}$ of this potential is a nonlinear variational parameter. The sensitivity to the parameter is very low (like one keV) in a wide range: $a_{(12)}\sim 3-8$ fm; see Sec. III. This shows high flexibility of our trial WF.

To avoid difficulties in solving systems of differential equations for nonorthogonal functions we should orthogonalize $\Psi^{(2)T}_{JM}$ to $\Psi^{(3)T}_{JM}$,

$$\Psi^{(2)T}_{JM,\text{ort}}=\Psi^{(2)T}_{JM}-\sum_{K=K^{(3)}_{\min},\gamma}^{K^{(3)}_{\max}}(\Psi^{(2)T}_{JM}|\mathcal{J}_{K,\gamma})\mathcal{J}_{K,\gamma}=\sum_i f_i(\rho)\mathcal{B}^{\text{ort}}_i(\mathbf{X},\mathbf{Y})\chi_{TM_T}. \quad (14)$$

[3]In our calculations we took it to be the same for neutrons and protons, equal to the average mass of nucleons.

From hereon in the brackets $(\cdots)$ for matrix elements denote integration over $d\Omega_5=\sin^2\theta\cos^2\theta\,d\theta\,d\Omega_x d\Omega_y$ and summation over spin variables.

To calculate matrix elements (MEs) of realistic binary (l-dependent, etc.) potentials we should expand our basis over eigenfunctions of angular momentum for each of three radii between particles. So to calculate matrix elements like $(\Psi^{(2)T}_{JM}|\hat{V}|\Psi^{T}_{JM})$ we are expanding $\Psi^{(2)T}_{JM}$ over the HH functions. This simplifies greatly all the expressions, but introduces another truncation in our calculation, namely, the number $K^{(2)}_{\max}$ of HHs effectively taken into account in the binary channel MEs. It also gives an opportunity to control the precision of ME calculations for a chosen maximal ρ value,

$$\Psi^{(2)}_{\rm ort}=\sum_i f_i(\rho)\sum_{K=K^{(3)}_{\max}+2,\overline{\gamma}_i}^{K^{(2)}_{\max}}\frac{\overrightarrow{\chi}^{\,1}_{K\overline{\gamma}_i}(\rho)}{\rho^{5/2}}\mathcal{J}_{K,\overline{\gamma}_i}(\Omega_5), \quad (15)$$

$$\overrightarrow{\chi}^{\,1}_{K\overline{\gamma}_i}(\rho)=\rho^{5/2}(\mathcal{B}_i|\mathcal{J}_{K,\overline{\gamma}_i}). \quad (16)$$

The overbar in $\overrightarrow{\chi}^{\,1}_{K\overline{\gamma}_i}(\rho)$ reminds us that it is a given function, unlike $\chi_{K,\gamma}(\rho)$ and $f_i(\rho)$, which have to be obtained as a solution of the Schrödinger equation. The multi-index $\overline{\gamma}_i=\overline{\gamma}_i(l_x,j_x,l_y,j_y)$ stands for the set of quantum numbers (QNs), which is specific to the binary channel number i, unlike the multi-index γ in Eq. (5), which formally runs over all possible sets of quantum numbers. As one can see from Eq. (10), the functions $\overrightarrow{\chi}^{\,1}_{K\overline{\gamma}_i}$, which have the same quantum numbers except j_y, differ only in a coefficient (it arises from $jj\to LS$ recoupling).

The WF Ψ^{T}_{JM} is a solution of the three-body Schrödinger equation:

$$(\hat{H}-E)\Psi^{T}_{JM}=0, \quad \hat{H}=\hat{T}+\hat{V}=\hat{T}+\hat{V}_{12}+\hat{V}_{23}+\hat{V}_{31}.$$

A set of coupled differential equations for the functions $\chi_{K,\gamma}(\rho)$, $f_i(\rho)$ is obtained using the ordinary variational procedure:

$$(\mathcal{J}_{K,\gamma}|\hat{H}-E|\Psi^{(3)}+\Psi^{(2)}_{\rm ort})=0,$$

$$(\mathcal{B}^{\rm ort}_i|\hat{H}-E|\Psi^{(3)}+\Psi^{(2)}_{\rm ort})=0.$$

When the hyperangular part of the WF is separated out, we obtain a set of coupled equations to determine $\chi_{K\gamma}(\rho)$ and $f_i(\rho)$, which are similar to equations of a single mass M particle motion in a deformed field:

$$\left[\frac{d^2}{d\rho^2}-\frac{\mathcal{L}(\mathcal{L}+1)}{\rho^2}-2M\{E_{3\rm sep}+V_{K\gamma,K\gamma}(\rho)\}\right]\chi_{K\gamma}(\rho)$$
$$=\sum_{\substack{K'=K^{(3)}_{\min},\gamma'\\ K',\gamma'\neq K,\gamma}}^{K^{(3)}_{\max}}2MV_{K'\gamma',K\gamma}(\rho)\chi_{K'\gamma'}(\rho)$$
$$+\sum_{i,\overline{\gamma}_i}E_{K\gamma,i\overline{\gamma}_i}(\rho)f_i(\rho), \quad (17)$$

$$\left[\frac{d^2}{d\rho^2}+A_i(\rho)\frac{d}{d\rho}+B_i(\rho)\right]f_i(\rho)=\sum_{i\neq i'}C_{i'i}(\rho)f_{i'}(\rho)$$
$$+\sum_{K'=K^{(3)}_{\min},\gamma'}^{K^{(3)}_{\max}}D_{K'\gamma'i}(\rho)\chi_{K'\gamma'}(\rho). \quad (18)$$

Here $\mathcal{L}=K+3/2$, and $V_{K'\gamma',K\gamma}(\rho)$ are standard hyperspherical MEs (see Appendix A for details):

$$V_{K'\gamma',K\gamma}(\rho)=\left(\mathcal{J}_{K'\gamma'}(\Omega_5)\left|\sum_{j\neq k=1}^{3}V_{jk}(\rho,\Omega_5)\right|\mathcal{J}_{K\gamma}(\Omega_5)\right).$$

The definitions of more complicated MEs (A_i, B_i, $C_{i'i}$, $D_{K'\gamma'i}$, $E_{K\gamma,i\overline{\gamma}_i}$) are given in Appendix B. In Eqs. (17) and (18) the functions $\chi_{K\gamma}(\rho)$ tend to zero[4] at large ρ, while

$$f_i(\rho)\overset{\rho\to\infty}{\to}\text{const}, \quad f_i'(\rho)\overset{\rho\to\infty}{\to}0. \quad (19)$$

Formally Eq. (19) arises from the asymptotic behavior of the MEs A_i and B_i:

$$A_i(\rho)\overset{\rho\to\infty}{\to}\text{const}, \quad B_i(\rho)\overset{\rho\to\infty}{\to}0.$$

The typical behavior of these MEs is shown in Fig. 1; the details of the computational procedure are discussed in Appendix A. In reality, as one can see from Fig. 1, that $B(\rho)$ approaches the asymptotic values slowly. It means that the asymptotic behavior (19) is reached at physically reasonable distances ($\sim$10 fm without and $\sim$20 fm with Coulomb interaction) due to the coupling of channels. We set $f(\rho)=\text{const}$ for $\rho<\rho_{\min}$, $f(\rho_{\min})=\text{const}$, and $f'(\rho_{\min})=0$. In practice, this does not put limits on the flexibility of our trial wave function due to the fact that $\Psi^{(2)}_{\rm ort}$ is extremely small at low ρ. This region of the WF does not influence the energy. No sensitivity to $\rho_{\min}$ can be found until $\rho_{\min}<0.6$–1.6 fm, depending on the other parameters.

[4]The functions $\chi_{\underline{K}\gamma}$ with the quantum numbers of the binary channel (namely, $\gamma=\gamma_i$) behave as $\overrightarrow{\chi}^{\,1}_{K\overline{\gamma}_i}$ at large ρ. For the other functions $\chi_{K\gamma}$ the boundary conditions (7) can be used.

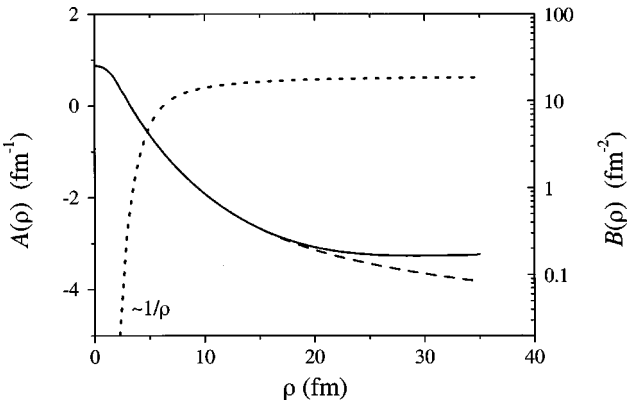

FIG. 1. Typical behavior of matrix elements in Eq. (18). Solid curve, $B_i(\rho)$ using Eq. (B2); dashed curve, $B_i(\rho)$ using Eq. (B6); dotted curve, $A_i(\rho)$. Calculations are performed for ^{6}Li with $K^{(3)}_{\max}=6$, $K^{(2)}_{\max}=50$.

Normally a few tens of equations (17) and as many equations (18) as the number of physical binary channels relevant to the problem are present. For example, for ^{6}Li only one extra equation (18) is required: that for a deuteron in relative s motion with the α particle. The most time-consuming part of the calculations is to obtain the expansion coefficients $\overrightarrow{\chi}^{-}_{K\gamma_i}(\rho)$ in Eq. (16). It can be done once during the computation for some trial energy $E_{2\text{sep}}$, or to improve the quality of the WF, it can be done continuously during the search for the bound state energy.

The spectroscopic factors $S_{j_x j_y}$ and ''radial spectroscopic functions'' $F_{j_x j_y}(Y)$ are defined as projections of the three-body WF onto the bound subsystem WF:

$$S_{j_x j_y}=\int |F_{j_x j_y}(Y)|^2 dY, \tag{20}$$

$$F_{j_x j_y}(Y)=\int [\psi_{l_x j_x}(\mathbf{X})\otimes[Y_{l_y}(\hat{Y})\otimes\chi_{S_3}]_{j_y}]_{JM} \times\Psi^T_{JM}(\mathbf{X},\mathbf{Y})d\Omega_x\, d\Omega_y Y X^2 dX. \tag{21}$$

They are used below to characterize the three-body WF in terms of a simple two-body representation.

The matter radius for a system mass A is $R^2_{\text{mat}}=(1/A)\Sigma_{i=1,\ldots,A}\langle R_i^2\rangle$, where R_i is the c.m. radius of nucleon i. For cluster systems it incorporates the experimental matter radii of the constituent clusters: 1.59(3) for triton, 1.74(5) for ^{3}He [17], and 1.46 for α particles [18].

III. ^{6}Li GROUND STATE

The $A=6$ nuclei are well studied with various approaches including the HH method [4,19]. Our purpose here is to verify the binary channel technique (or interpolation approach) before we apply it to more complicated cases, such as, for example, the ^{8}B nucleus. Therefore we simplified the potentials to obtain ^{6}Li characteristics reasonably well from one side and to avoid complicated calculations from another side.

What we are going to demonstrate in this section is that in the presence of long-range binary correlations the convergence of the radius is slower than the convergence of the binding energy. In the ordinary HH method it could lead to a situation where the feasible basis size is not sufficient to describe radial properties precisely, while in the IA method the convergency of both energy and radius is achieved.

Following Ref. [4] the potential $V_{\alpha N}$ was chosen similar to that in Ref. [20], but with a larger radius, which makes it possible to reproduce well many characteristics of the $A=6$ nuclei in HH calculations. The effect of this variation of the radius on the α-N phases is described in [7]. The potential is of the form

$$V_{\alpha N}(R)=V_C(R)+(\mathbf{LS})V_{LS}(R),$$

$$V_C(R)=V^l_C\ \exp[-(R/R_0)^2], \tag{22}$$

$$V_{LS}(R)=V^l_{LS}\ \exp[-(R/R_0)^2],$$

with $R_0=2.35$ fm. The strengths of the potential depend on the relative αN angular momentum l: $V^0_C=50.0$ MeV, $V^1_C=-47.32$ MeV, and $V^2_C=-23.0$ MeV; $V^1_{LS}=V^2_{LS}=-11.71$ MeV. Components with higher angular momenta are put to zero. The potential is repulsive in the s wave, which takes account of the Pauli principle. A pointlike Coulomb interaction was also included. The NN interaction was taken to be a simple central potential, acting only in the s wave [14]:

$$V_{np}(R)=-66.92\exp[-(R/1.55)^2].$$

It gives the deuteron binding energy $E_x=2.170$ MeV and rms radius 1.97 fm. In the present calculation the binary channel function (8) consists of the s-wave deuteron cluster in a relative s state with the α particle and one equation for the function $f_{\{0100\}}(\rho)$ is added to the ordinary set of HH equations (the results of more advanced standard HH calculations with a realistic NN potential are given, for example, in Ref. [4]).

Figure 2 represents the trends of convergence of the binding energy and the matter radius in the case of an ordinary HH calculation. The convergence of the binding energy is practically achieved at $K=12$, and E_{12} differs by 2% from the asymptotic value, given by Eq. (23). On the contrary, there is no obvious convergence for the matter radius, although the range of its variations is about 0.1 fm. The asymptotic binding energy of the system can be evaluated as

$$E_{\text{as}}=\frac{E_K E_{K-4}-E^2_{K-2}}{E_K-2E_{K-2}+E_{K-4}} \tag{23}$$

using the exponential character of the energy convergence for Gaussian potentials in the HH method. For $K=12$, $E_K=-3.91$ MeV, and the asymptotic energy is -3.98 MeV.

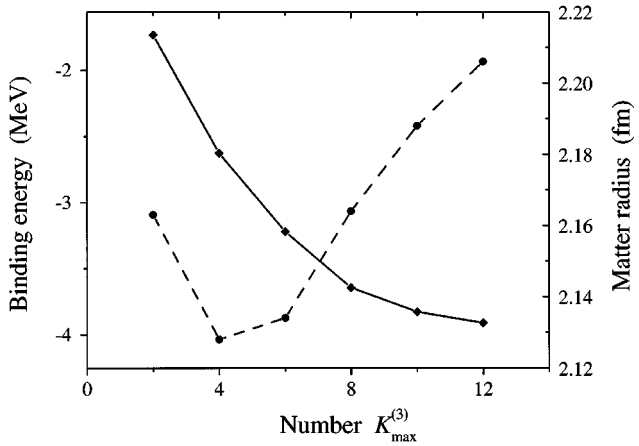

FIG. 2. Dependence of binding energy (solid line, diamonds) and matter radius (dashed line, circles) on maximal hypermomentum $K^{(3)}_{max}$ in the ordinary HH method. Potentials are given in Sec. III.

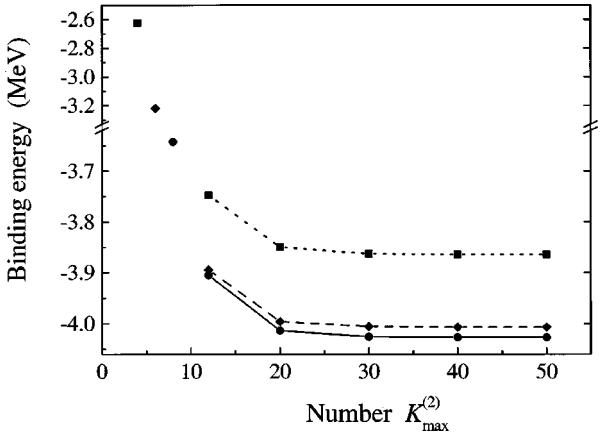

FIG. 3. The convergence curves for binding energy in the HH method with the binary channel included. $K^{(2)}_{max}$ is the number of *effective* hyperspherical harmonics taken into account in the binary channel (this value controls the quality of the ME calculations at large ρ). Convergence is practically achieved at $K^{(2)}_{max}\sim 30$. Different curves correspond to different numbers $K^{(3)}_{max}$ of the basis hyperspherical harmonics taken into account. Squares, diamonds, and circles correspond to $K^{(3)}_{max}=4$, 6, and 8, respectively. The lines are given only to guide the eye. To demonstrate the improvement in comparison with ordinary HH calculations three points obtained without the inclusion of the binary channel are given separately: $K^{(3)}_{max}=4$ (square), $K^{(3)}_{max}=6$ (diamond), and $K^{(3)}_{max}=8$ (circle).

Some very small components of the WF are neglected in this calculation. In the case of ^{6}Li, the main contributions to the three-body WF arise from channels with quantum numbers of the deuteron and the *s*-wave α-*d* relative motion. This has transparent physical meaning. For low K values it is connected with the ''Pauli focusing effect;'' see [21]. For higher K values this can be understood as follows. The larger the K value, the larger is the characteristic ρ described by this HH. When the ρ value becomes large, the ''democratic'' three-body configurations with the ''short'' asymptotic (7) vanish, and only the $\alpha+d$ structure with the ''long'' asymptotic (12) survives. Dominance of ''deuteronlike'' correlation is caused by its energy efficiency, but to obtain it in the HH method we need very many HHs with deuteron quantum numbers. Thus a practical way to move far in K value in HH calculations for a ''non-Borromean'' system is the following: starting from some K value to retain only HHs with quantum numbers corresponding to the clusterization of a system.

The fact that at K values larger than some $K>K^{(3)}_{max}$ only the α-*d* asymptotics contributes significantly to the binding energy can be verified in the following way. We performed ordinary HH calculations with $K^{(3)}_{max}=8$. The results are shown in the first row of Table I. Then we increased $K^{(3)}_{max}$ up to 14, but for $K^{(3)}_{max}>8$ we included only harmonics with quantum numbers, corresponding to the binary channel. The results are demonstrated in the second row of Table I (marked by ''HH+tail''). The calculations of the third type were done with the binary channel (or IA) technique for $K^{(3)}_{max}=8$, $K^{(2)}_{max}=50$. The results are shown in the third row of Table I and marked by ''HH+BC.'' If we compare the results of ''HH+tail'' and ''HH+BC'' calculations with pure HH ones, we immediately see that the α-*d* asymptotics is very important and contributes substantially to the binding energy. If we compare ''HH+tail'' with ''HH+BC'' results, we can see that the single binary channel provides a larger binding energy than six three-body channels with the quantum numbers of the binary channel. This means that the suggested method works well even in the ^{6}Li case, where the separation energy of the α particle is only slightly smaller than the binding energy of the deuteron. It is also seen from Table I that IA leads to a larger size of the ^{6}Li nucleus (while the distance between valence nucleons r_{NN} decreases).

TABLE I. Binding energies E_{3sep} in MeV and geometrical characteristics in fm of the ^{6}Li nucleus, obtained in calculations of three different kinds. For details, see the text. Here R_{mat} is the matter radius, r_i is the rms distance between a particle $i=\{\alpha,N\}$ and the center of mass, and r_{ij} is the rms distance between particles i and j.

^{6}Li	E_{3sep}	R_{mat}	r_N	r_α	r_{NN}	$r_{N\alpha}$
HH	3.642	2.164	2.729	1.081	3.331	3.646
HH+tail	3.906	2.204	2.786	1.127	3.278	3.757
HH+BC	4.027	2.286	2.914	1.209	3.255	3.974

Figures 3 and 4 refer to the case of the BC calculation. They show how many basis HHs in the three-body channels should be retained ($K^{(3)}_{max}=4,6,8$) and the effective harmonics included in the binary channel ME calculation to obtain the energy and matter radius. These curves correspond to the parameters $a_{(12)}$ giving the minimal energy for fixed $K^{(3)}_{max}$: ($K^{(3)}_{max}=4$, $a_{(12)}=3.0$), ($K^{(3)}_{max}=6$, $a_{(12)}=3.8$), ($K^{(3)}_{max}=8$, $a_{(12)}=4.0$). Everywhere $l_x(\max)=l_y(\max)=2$. We see that $K^{(3)}_{max}=8$, $K^{(2)}_{max}=20$–30 is enough for complete energy convergence. But in order to describe the WF precisely at large distances one should increase $K^{(2)}_{max}$ up to 40–50. This does not lead to a large increase in the number of the effective harmonics since only HHs with specific l_x, l_y, and L

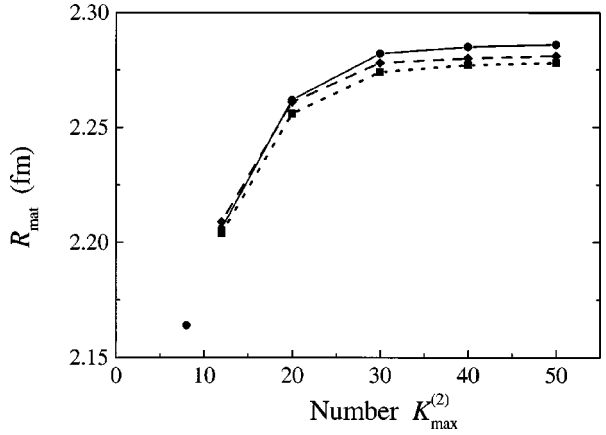

FIG. 4. The convergence curves for matter radii with the binary channel included. $K^{(2)}_{max}$ is the number of the *effective* hyperspherical harmonics taken into account in the binary channel ME. Different curves correspond to different numbers of hyperspherical harmonics taken into account in the ''ordinary'' three-body channels. The notation is the same as in Fig. 3. The convergence of the matter radius is achieved only for $K^{(2)}_{max}\sim 40-50$.

enter the expansion (15). For $K^{(2)}_{max}\leqslant 12$ the BC calculation results (Figs. 3 and 4) coincide practically with the ordinary HH results shown in Fig. 2 for corresponding $K^{(3)}_{max}=K^{(2)}_{max}$. So Figs. 3 and 4 could be considered as an extension of Fig. 2 to higher K values.

The characteristic sensitivity of the binding energy and the matter radius to the nonlinear variational parameter $a_{(12)}$ is shown in Fig. 5. For practical purposes we can take any value of $a_{(12)}$ in a wide range (3–8 fm).

The following conclusion can be drawn from the studies of the ^{6}Li ground state. Taking into account the physical peculiarities of the system, namely, the asymptotic formation of the deuteron cluster in ^{6}Li, the method allows us to achieve a fast energy convergence, solving even very few HH equations (Fig. 3). The convergence of the radial characteristics is also very rapid if the binary channel MEs are calculated with good precision (Fig. 4, $K^{(2)}_{max}\geqslant 40$).

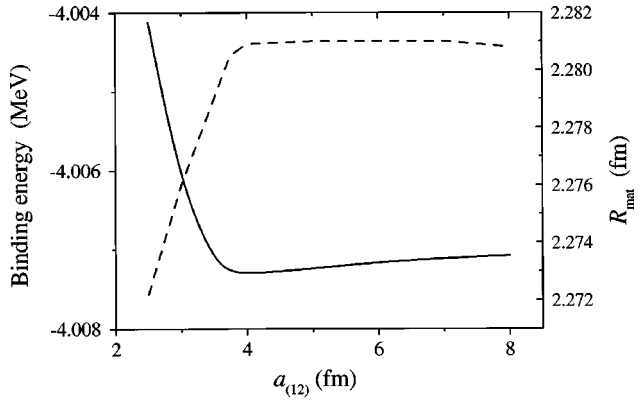

FIG. 5. Binding energy (solid curve) and matter radius (dashed curve) as functions of the nonlinear variational parameter $a_{(12)}$. The quality of the suggested variational function in the BC method is manifested in the high stability of the binding energy as well as the matter radius to this parameter. Calculations are performed with $K^{(3)}_{max}=6$, $K^{(2)}_{max}=50$.

It should be noted that the value obtained for R_{mat} in the ordinary HH calculations with a realistic *NN* potential is $R_{mat}\sim 2.35$ fm (for $K^{(3)}_{max}=12$ [4]). It is at the lower limit of the experimental value 2.4 ± 0.05 fm [22]. With our simple *NN* potential we get $R_{mat}\sim 2.2$ for $K^{(3)}_{max}=12$ in pure HH calculations. Calculations with the BC gave ~ 2.29 fm. Together with an overestimation of the binding energy, contracting the system, this makes us think that using the same approach with a realistic *NN* potential it would be possible to reproduce R_{mat} for ^{6}Li rather well.

IV. MODEL WITH A REDUCED α-*N* INTERACTION

The ^{6}Li nucleus is not the most suitable case for application of the binary channel technique. The separation energy of the deuteron cluster is ~ 1.8 MeV in our calculation, while the binding energy of the deuteron is ~ 2.2 MeV. The difference of these energies is small and close to the limit of ''rigorous'' applicability of the method [see Appendix B, Eq. (B5)]. The sizes of the deuteron and α-*d* relative motion WFs are comparable and therefore it is possible to expand the WFs over a reasonable number of HHs (see Table I). In three-body systems like ^{8}Be, the two-body cluster separation energy is low in comparison with the binding energy of a cluster. This makes the ordinary HH method practically inapplicable, as it requires a tremendous number of HH equations to be solved to reproduce the binary cluster asymptotic at large distances, as already mentioned in the Introduction.

The binary channel formalism was developed to deal with such three-body systems, with subsystems loosely bound with respect to the two-body threshold. In the previous section the method was verified in a well-investigated situation. Now we want to check how well it works in the case of a loosely bound cluster in the model situation of ''nucleon weakly interacting with an α particle.''

In the potential (22) we reduce the main component responsible for binding, putting $V^1_C=-41.5$ MeV. The radial spectroscopic functions $F_{10}(Y)$ [i.e., the overlaps (21) with the deuteron WF] for the ^{6}Li WF of the preceding section and for the ''^{6}Li'' WF obtained with a modified potential are shown in Fig. 6. It is seen that for the case of a smaller α-*d* separation energy the probability of finding a deuteron at large distances increases substantially. In Fig. 7 the convergence curves for the binding energy and the radius are shown. The set of parameters adopted in these BC calculations is ($K^{(3)}_{max}=8$, $a_{(12)}=4.0$, $l_x(\max)=l_y(\max)=2$). The deuteron separation energy E_y is found to be 87 keV. Performing an ordinary HH calculation, we retain all HHs with $K^{(3)}_{max}\leqslant 8$, $l_x(\max)=l_y(\max)=2$ and only HHs with the deuteron quantum numbers at higher K values. In this calculation we were unable to go further than up to $K^{(3)}_{max}=20$. We can, however, decrease $K^{(2)}_{max}$ in the BC calculation, to see the consistency of the two approaches (the HHs with BC quantum numbers play the same role as the corresponding BC function components). For $K^{(2)}_{max}<30$ the E_{3sep} energy is smaller than the deuteron binding energy $E_x=2.17$ MeV, so

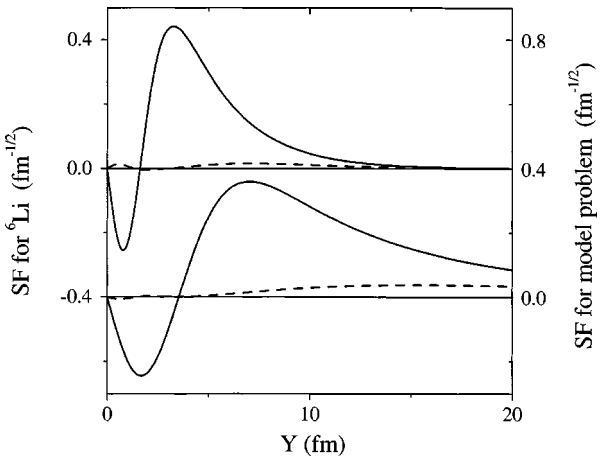

FIG. 6. Radial spectroscopic functions (21) for d in ^{6}Li (left axis, upper part of the figure) and for d in the model system with a reduced α-N interaction (right axis, lower part of the figure). Calculations are performed with $K^{(3)}_{\max}=6$, $K^{(2)}_{\max}=50$. Dashed curves show the fraction of spectroscopic function connected with the binary channel.

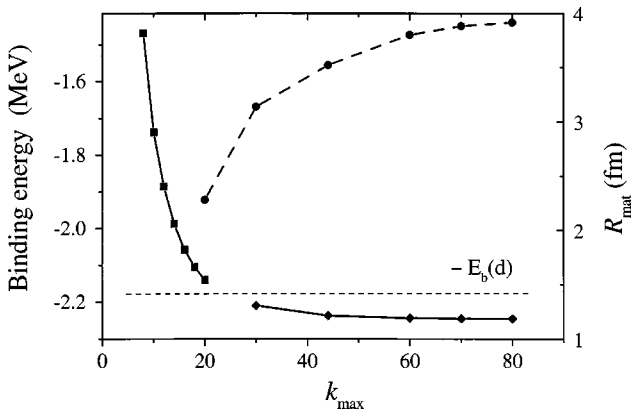

FIG. 7. Convergence of binding energy (solid curves) and matter radius (dashed curve) for the model problem ''^{6}Li with a reduced α-N interaction.'' The quantity $k_{\max}$ is $K^{(3)}_{\max}$ for HH calculations and $K^{(2)}_{\max}$ for BC calculations. Squares stand for both pure HH calculations and BC results with $K^{(2)}_{\max}<30$; diamonds for BC results for $K^{(2)}_{\max}\geqslant 30$, and circles for the matter radius.

the $\alpha+d$ subsystem is unbound, but expression (13) formally allows it.[5] The points for the energy convergence of the BC calculations are not shown separately in Fig. 7 for $K^{(2)}_{\max}<30$ because they just coincide within 0.5 keV with the points for the HH calculations.

The binding energy gained by adding the binary channel to the ''complete'' $K^{(3)}_{\max}=8$ calculation (29 channels together) is about 800 keV. This effect of the BC is not so drastic in comparison with $K^{(3)}_{\max}=20$ ordinary HH calculations (only channels with deuteron quantum numbers are accounted for, $K^{(3)}_{\max}\geqslant 10$, 35 channels in total): only $\sim$130 keV. But here this energy gain allows us to get a binding energy of the three-body system larger than the deuteron binding energy (hence to move under the two-body breakup threshold) and obtain good energy convergence and a reliable WF. The ordinary HH method is good here only for evaluation purposes, until we are able to move to $K^{(3)}_{\max}$ $\sim$30–40. Note that $R_{\rm mat}$ is essentially larger in that case, compared with previous calculation (Fig. 4), and needs a larger $K^{(2)}_{\max}\sim$60–80 for convergence.

V. STRUCTURE OF THE ^{8}Li AND ^{8}B NUCLEI

This subject was discussed in brief in our previous paper [2]. Here both the convergence of the calculations and the physical aspects of the results are considered which were not elucidated in [2].

The parameters for Woods-Saxon (WS) and Gaussian type intercluster potentials we use are listed in Table II. The potentials include central, SS, and LS terms. In the WS case the potentials are of the form

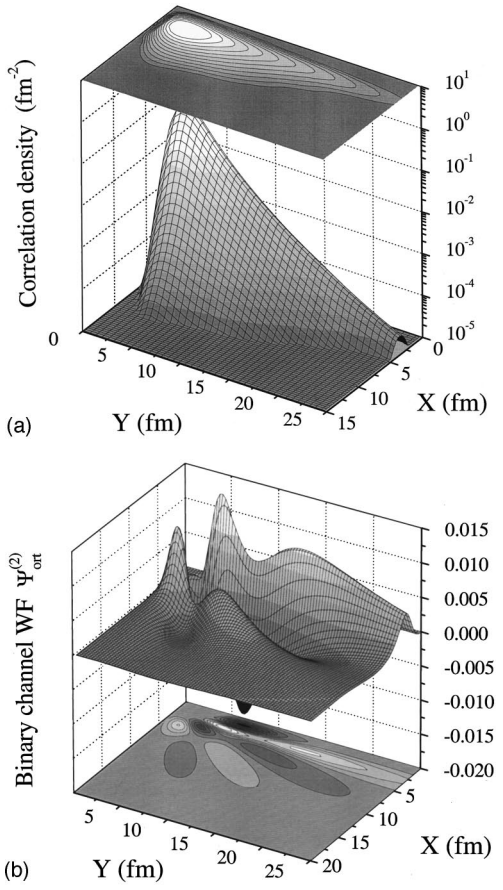

FIG. 8. Correlation density for the total WF $\Psi^{(3)}+\Psi^{(2)}_{\rm ort}$ (a) and the binary channel function $\Psi^{(2)}_{\rm ort}$ (b) for ^{8}B. Here Y is the distance between p and the c.m. of ^{7}Be. Note that the total WF is smooth. The complicated spatial behavior of $\Psi^{(2)}_{\rm ort}$ at intermediate distances is connected with the orthogonalization procedure (14). From the physical point of view it is required to provide the correct asymptotic behavior of the WF in the regions of space where $\Psi^{(3)}$ fails to reproduce the correct asymptotic (for the fixed $K^{(3)}_{\max}$ value).

[5]Over the two-body threshold the asymptotic (13) for the BC function (8) is physically irrelevant. Nevertheless, function (8) plays a good role as the variational term.

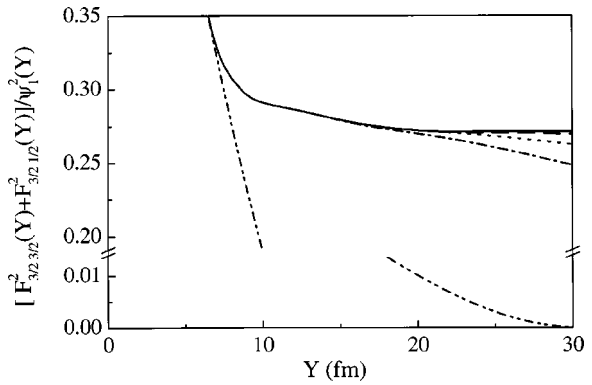

FIG. 9. Convergence of the full WF to the binary channel WF for ^{8}B when the precision of the BC MEs is increased. The solid, dashed, dotted, and dash-dotted curves correspond, respectively, to $K^{(2)}_{\max}=70$, 60, 50, and 40. The pure three-body calculation (no binary channel) is represented with a dash-double-dotted curve.

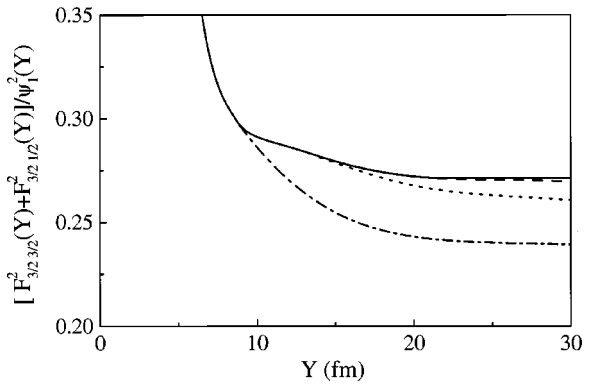

FIG. 10. Convergence of the ^{8}B WF binary asymptotic when the three-body basis is increased. The solid, dashed, dotted, and dash-dotted curves correspond, respectively, to $K^{(3)}_{\max}=12$, 10, 8, and 6. $K^{(2)}_{\max}=60$ in all cases.

$$V_{C,SS}(r)=\sum_i \frac{V_i^l}{1+\exp[(r-r_i^l)/a]},$$

$$V_{LS}(r)=\frac{V_0^l \exp[(r-r_0^l)/a]}{r(1+\exp[(r-r_0^l)/a])^2}. \tag{24}$$

The potentials reproduce well observables in binary subsystems, as described in Ref. [1]. Coulomb potentials (A3) of a homogeneously charged sphere are used. Radii of the spheres are determined by the charge radii of the clusters: $r^2_{0ij}=5[r^2_{\rm ch}(i)+r^2_{\rm ch}(j)]/3$, $r_{\rm ch}(p)=0.8$ fm, $r_{\rm ch}(^3{\rm H})=1.72(9)$ fm, $r_{\rm ch}(^3{\rm He})=1.93(5)$ fm [17], and $r_{\rm ch}(\alpha)=1.67$ fm [18].

One of the important issues concerned in [2] was the calculation of the astrophysical factor $S_{17}(0)$ by means of the asymptotic normalization coefficients method [23,24]. This question is closely connected with the problem of the radial convergence of the calculations. A rather slow convergence of the three-body WF to the binary asymptotics in the case of the strong three-body Coulomb interaction (say, ^{8}B, in contrast with ^{8}Li) was found in Ref. [2]. Now we are going to discuss this problem.

The main part of the variational calculation [2] for the 2^+ ground state (g.s.) consists of 42 channels with $K^{(3)}_{\max}=6$. It includes all possible sets of quantum numbers up to $L=3$, $l_x=3$, and $l_y=3$. Complete energy convergence is achieved if we add to it 9 channels with quantum numbers of BC ($^7{\rm Be}+p$ in the p wave) up to $K^{(3)}_{\max}=12$. However, this is not enough if we want to go quite far in the ρ value to calculate MEs for electromagnetic transitions or such a subtle ''observable'' for g.s. WF as $S_{17}(0)$ value. The geometry of our ^{8}B WF is shown in Fig. 8. In Figs. 9–11 we study the accuracy with which our calculations reproduce the true behavior of the WF at large Y. The squared ratio[6] of the spectroscopic function (21) and the BC relative motion function (12) are chosen to demonstrate various aspects of convergence in Figs. 9–11. The following points should be emphasized.

(i) The pure three-body HH method WF does not allow one to reproduce binary asymptotics at large distances (very many terms should be retained to reproduce large Y behavior). The dash-double-dotted curve in Fig. 9 shows HH calculations with $K^{(3)}_{\max}=12$, where all HHs up to $K^{(3)}_{\max}=6$ and only HHs with quantum numbers of the binary channel for $K^{(3)}_{\max}>6$ are included. At $Y>8$ fm the true behavior of the WF is not reproduced.

(ii) The MEs of the binary channel should be calculated with a high enough precision (number $K^{(2)}_{\max}$) for a chosen ρ value. The higher is the Y value, the more HHs in the expansion of the BC component of the WF should be retained. Figure 9 demonstrates that increasing $K^{(2)}_{\max}$ we increase the distance at which the calculation is exact. If the line tends to a constant in some range of Y, then we do not need to increase the precision of ME calculations any more as the real binary asymptotic is achieved.

(iii) The solid curve in Fig. 9 demonstrates that MEs of the BC were calculated well enough up to $\rho\sim 25$ fm ($Y\sim 26.4$ fm) with $K^{(2)}_{\max}=60$. Figure 10 shows calculations

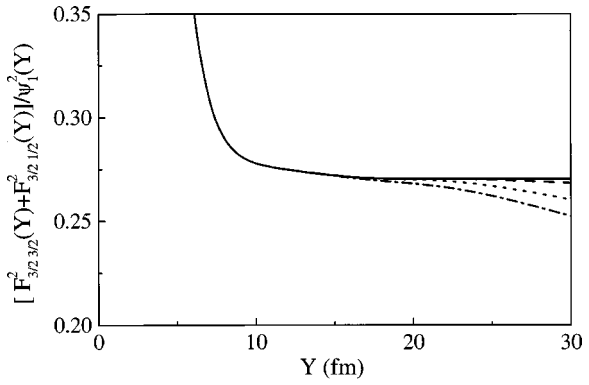

FIG. 11. The same as Fig. 9, but for the model problem with no Coulomb interaction in the binary channel. The ''proton'' separation energy is the same as in ^{8}B.

[6]This value is proportional to $S_{17}(0)$ for large Y.

TABLE II. Parameters of the potentials used in the calculations of ^{8}Li and ^{8}B (here and in Ref. [2]). The α-''t'' potential is parametrized in Gaussian form (22). For ''t''-N and α-N potentials the WS form (24) is used. ''t''-N and α-''t'' potentials have a repulsive term, as well as an attractive term, put in a separate column. Each cell contains depth V_i^l and width r_i^l parameters for one potential term. The diffusiness parameters a of the WS potentials are 0.7 fm for the central and SS components and 0.35 fm for the LS component.

Term	l	''t''-N, WS				α-''t'' (Gaussian)				α-N (WS)	
		V_0^l	r_0^l	V_1^l	r_1^l	V_0^l	r_0^l	V_1^l	r_1^l	V_0^l	r_0^l
Central	s	−33.0	2.0	350.0	1.43	−122.2	2.1	400.0	1.75	43.0	2.0
	p	−35.0	2.0			−141.6	2.1	300.0	1.43	−43.0	2.0
	d	−33.0	2.0	350.0	1.43					−7.0	2.0
	f	−35.0	2.0			−48.52	3.1				
LS	p	−56.0	1.5			−2.3	2.1			−114.29	1.5
	d	−56.0	1.5							−114.29	1.5
	f	−56.0	1.5			−13.2	1.91				
SS	s			200.0	1.43						
	p	−2.7	2.0								
	d			200.0	1.43						
	f	−2.7	2.0								

with this value of $K_{\max}^{(2)}$ but with $K_{\max}^{(3)}=6,8,10,12$. This figure illustrates why the method is called the *interpolation approach*: the three-body basis we are using should be wide enough to interpolate successfully the ''intermediate'' region in the space, where the asymptotic of the WF is transferred from the three-body one to the binary one.

(iv) The binary asymptotics for ^{8}B is commonly believed to be achieved at the distances $Y\sim 5-8$ fm (see, for example, [23]). One can find in Fig. 9 that in our method complete convergence to the binary asymptotic takes place at about 22–25 fm. We have done the special calculation with the Coulomb interaction switched off in the α-p and ''t''-p subsystems to find out if this is not an artifact of our method. Simultaneously the short-range strong interactions were made less attractive to keep the ''proton'' separation energy for ''^{8}B'' around the experimental value. Although all other global properties of the system are practically the same, the exponential asymptotics for the binary channel in this case is reached at essentially smaller distances (see Fig. 11) than the Coulomb asymptotics in the ^{8}B case. This result shows that one should calculate WFs for larger distances if the three-body Coulomb interaction is present.

Table III demonstrates the sensitivity of observables for ^{8}Li and ^{8}B to the maximal radius $\rho_{\max}$ they are calculated for.[7] For ^{8}Li the observables are saturated at $\rho_{\max}\sim 10$ fm. For bulk properties of ^{8}B larger distances up to $\rho_{\max}\sim 15$ fm are important. Those observables, which are sensitive to the asymptotics $[|R_n-R_p|,Q,S_{17}(0)]$ stabilize only at $\rho_{\max}\sim 21-25$ fm. At $\rho_{\max}\sim 15$ fm their deviations from final result are around 10%.

Table IV shows the contributions of each cluster in the quadrupole and magnetic moments. The most serious discrepancies for observables in [25,26] are those for magnetic moments: the theoretical value for ^{8}B is close to experimental values in ^{8}Li and vice versa. In our previous calculations [2] the discrepancy is much lower. As was discussed in [2] those better results were obtained due to the use of experimental magnetic moment values for ^{3}H and ^{3}He clusters ($2.98\mu_N$ and $-2.13\mu_N$, respectively). In Refs. [25,27,26] simple single-Gaussian WFs for ^{3}H and ^{3}He clusters are used and hence the magnetic moments associated with these clusters are close to single-particle ones ($2.79\mu_N$ and $-1.91\mu_N$). If we substitute single-particle values in our calculations, then we obtain $\mu(^8\text{Li})=1.16$ and $\mu(^8\text{B})=1.60$ which are close to those in [25,26] ($\mu(^8\text{Li})=1.18,\ 1.17$, $\mu(^8\text{B})=1.61,\ 1.42$). It is easy to find out that with $\mu(^3\text{H})=3.28$ and $\mu(^3\text{He})=-2.47$ the experimental magnetic moments of ^{8}B and ^{8}Li are reproduced. This allows us to speculate about the possible polarization of ''t'' clusters in the g.s. WFs of $A=8$ nuclei. Such a polarization does not destroy the three-cluster picture we use as only a few more percent of a d-wave admixture in $A=3$ clusters is sufficient to change the magnetic moment this way. On the other hand, if this guess is correct, then to describe such observables as μ for $A=8$ nuclei we need a RGM-like model with realistic interactions, treating s and d waves in triton dynamically.

We also estimated the positions and spectroscopic factors for various states in ^{8}Li and ^{8}B. Calculations were done with bound state or three-body quasiresonant boundary conditions (for details of the quasiresonant formalism see [21]). Table V summarizes these results. The structure information in Table V is given in terms of jj coupling. This resembles the shell-model language as the outer neutron (proton) is in a state with a definite total angular momentum (j_y) with respect to the c.m. of the system. It is preferable to present the structure information in this form, though it is well known that light nuclei ''prefer'' LS coupling. In $A=8$ this preference can be seen as the strong domination of one (maximum two) components in the WF in LS coupling.

The 2^+ ground state in ^{8}Li and ^{8}B is dominated by the $(LS\ l_x l_y)=(1111)$ component—97%. However, about 20 other components are required to obtain energy convergence.

[7] If $\rho_{\max}>6$ fm, then $\rho_{\max}\approx\sqrt{7/8}Y_{\max}$.

TABLE III. Sensitivity of various observables in ^{8}Li (left part) and ^{8}B (right part) to the radius of integration, $\rho_{\max}$. The symbol ∞ denotes stability of the results. The values in the table are calculated for the two-body separation energies adjusted to be exactly experimental.

$\rho_{\max}$	7.5	10	15	∞	7.5	10	15	∞
$R_{\rm mat}$	2.24	2.35	2.38	2.38	2.26	2.46	2.56	2.59
R_n	2.30	2.44	2.48	2.48	2.15	2.27	2.30	2.31
R_p	2.12	2.19	2.21	2.21	2.33	2.57	2.70	2.75
$\lvert R_n - R_p \rvert$	0.18	0.25	0.27	0.27	0.18	0.30	0.40	0.44
$Q(\mathrm{fm}^2)$	1.84	2.07	2.11	2.11	3.96	5.19	6.08	6.52
μ (μ_N)	1.26	1.34	1.35	1.35	1.19	1.33	1.34	1.38
$S_{17}(0)$					21.0	20.8	20.0	19.2

The 1^+ states are the orthogonal mixture of $S=0$ and $S=1$ components. The lower state consists of (1011), 83% and (1111), 15%; the upper state has the inverse corresponding weights. The higher 1^+ level is known to have a broad width. We recall that the two-body decay properties of the states were not considered in our calculations.

The 3^+ is seriously mispositioned in our calculations. This state is underbound and modification of the high angular momentum components of potentials, which are not well determined experimentally, does not improve the situation. It makes us think that the state is falling outside of our model space. The following experimental facts support this point of view: (i) low experimental spectroscopic factors for neutron (proton) scattering on ^{7}Li (^{7}Be) as compared to those calculated in our model and (ii) the Coulomb shift is higher for 3^+ state ($\Delta E=2.04$ MeV) than for 2^+ or 1^+ ($\Delta E=1.98$, 1.77 MeV) as we turn from ^{8}Li to ^{8}B. It should mean that 3^+ is more compact than 2^+ or 1^+, which is easily understood if 3^+ is not a cluster state, like 2^+ or 1^+, but a ''compound nucleus'' state.

The position and width of the 4^+ in ^{8}Li were reproduced well. The structure is dominated by a neutron in the f wave (4113), 45% and (4013), 32%. This is what we would expect from the binary model considering the low width of the state. Nevertheless, there is a significant component with the f wave in α-t relative motion (3131) ''built'' upon the f-wave states in ^{7}Li. The decay width to the three-body continuum (with the energy of the state adjusted to the exactly experimental value) is ~ 45 keV. It is compatible with the experimental width of the state (35 ± 15 keV) unlike the width of binary f-wave neutron emission, which requires quite a low spectroscopic factor (~ 0.06–0.14) for a realistic radius of the channel.

The spectroscopic factors $S_{j_x j_y}$ as well as the radial spectroscopic functions (21) are especially important for estimates of different reactions involving these nuclei in initial or final states, for example, nucleon capture on ^{7}Li and ^{7}Be nuclei, nuclear fragmentation, and Coulomb dissociation of ^{8}Li and ^{8}B. It is seen from Table V that the excited states of the ^{7}Li and ^{7}Be cores give essential contributions to spectroscopic factors, especially for 1^+ states.

There are numerous fingerprints, both experimental and theoretical, of negative parity states in ^{8}Li and ^{8}B [28–30]. These states can be seen as s waves in neutron (proton) scattering, and if they are situated far from the binary threshold, their signatures become too indefinite for clear experimental identification. Without further details, we got the 2^-, 1^-, 0^- ordering for negative parity states in both ^{8}Li and ^{8}B.

The overall quality of the approach to the spectrum of $A=8$ nuclei is reasonably high considering the uncertainties of experimental knowledge. Not all of the states in the spectrum (3^+) are within the scope of the model. Also, calculation of magnetic moments requires renormalization of the cluster properties. For all the other values being calculated (see also [2]), the model did not face severe problems.

VI. CONCLUSION

Techniques for explicitly incorporating two-cluster correlations into the three-cluster description of light nuclei have been developed here in the framework of the hyperspherical approach. This enables us to deal with three-body systems where two-body and three-body thresholds are close to each other while the two-body threshold is the lowest one. In this way the main effects of the strong deformation and dynamical polarization of the two-body cores as well as the core excitations are treated simultaneously.

Already in the case of systems like ^{6}Li, where the removal energy of the two-nucleon cluster is comparable to the two-nucleon binding energy, our method allows us to obtain a faster energy convergence and a larger binding energy than

TABLE IV. Partitions for quadrupole and magnetic momenta. The values $q_i=\langle (R_z^{(i)})^2 \rangle_{M_Z=J}$ give an additional insight into the quadrupole deformation associated with individual clusters, providing comparable values for all three clusters in ^{8}Li and ^{8}B; $Q=\Sigma_{i=N,\alpha,t} Z_i q_i$.

Nucleus	q_N (fm^2)	q_α (fm^2)	$q_{\cdot\cdot t\cdot\cdot}$ (fm^2)	μ_N(orb)	μ_α(orb)	$\mu_{\cdot\cdot t\cdot\cdot}$(orb)	μ_N(spin)	$\mu_{\cdot\cdot t\cdot\cdot}$(spin)
^{8}Li	1.82	0.573	0.965	0.0	0.120	0.101	-1.843	2.975
^{8}B	3.39	0.586	0.977	0.466	0.121	0.204	2.708	-2.120

TABLE V. Dominating spectroscopic factors for the ^{8}Li and ^{8}B WFs. Calculated excitation energies $E_{\rm exc}$ are given from the ground state energies (calculated three-body separation energies are 4.647 and 1.874 MeV for the g.s. of ^{8}Li and ^{8}B correspondingly). Experimental energies are from [22], except the energy of the second 1^+ state in ^{8}B, which is from [31].

State	j_x, j_y	$E_{\rm exc}$	E(expt)	$S_{j_xj_y}(^8{\rm Li})$	$E_{\rm exc}$	E(expt)	$S_{j_xj_y}(^8{\rm B})$
2^+	1/2 3/2	0.0	0.0	0.158	0.0	0.0	0.156[a]
	3/2 1/2			0.092			0.101
	3/2 3/2			0.667			0.685
1^+	1/2 1/2	1.091	0.981	0.121	0.882	0.77	0.124
	1/2 3/2			0.343			0.333
	3/2 1/2			0.002			0.003
	3/2 3/2			0.483			0.495
1^+	1/2 1/2	1.98	3.21	0.03	2.05	$\sim$3.0 [31]	0.04
	1/2 3/2			0.28			0.24
	3/2 1/2			0.56			0.57
	3/2 3/2			0.10			0.12
3^+	3/2 3/2	3.87	2.255	0.95	2.97	2.32	0.88
4^+	1/2 7/2	6.77	6.53	0.65	5.85		0.60

[a]This value was given erroneously in Refs. [2,33] as 0.083. However, it does not influence the results and conclusions of Ref. [2] and changes the results of Ref. [33] only slightly.

the most extensive HH calculations done so far without the two-cluster component. In addition, in the case of three-cluster systems with small removal energy of the two-body cluster, when the latter type calculations become quite lengthy, our approach remains appropriate. It has been demonstrated in this paper that when the removal energy is very small, and the ordinary HH calculation runs into problems, our approach works quite well.

We have applied the approach to study the structure of the ^{8}Li and ^{8}B nuclei considered as three-cluster $\alpha+{}^3{\rm H}({}^3{\rm He})+N$ systems. Ground state properties, such as neutron, proton, and matter radii, quadrupole and magnetic moments, and the asymptotic normalization constant, have been considered. In particular, the shortcomings of the three-cluster model for a description of the magnetic moments have been discussed. Level positions and spectroscopic factors of various configurations in the ground and excited states have been obtained. The three-cluster model was found to provide a good overall description of experimental data. We note that our values of the spectroscopic factors of the ^{8}B g.s. wave function have obtained an experimental confirmation in the experiment on Coulomb breakup of ^{8}B [32]. The ^{8}B wave function has also been successfully used for estimations of the ^{7}Be momentum distributions from recently measured ^{8}B fragmentation on a carbon target at high energy [33].

Three-cluster states in the ^{8}Be nucleus can also be investigated in the framework of our model. An approach similar to that used in the present paper may also be applied for studying the two-body continuum in a three-cluster system. For this purpose only the asymptotic behavior of the BC components of a WF should be modified.

ACKNOWLEDGMENTS

B.V.D. and N.B.S. thank Chalmers University of Technology for support and hospitality. L.V.G. and B.V.D. thank the Royal Swedish Academy of Science for financial support. Support from Russian RFBR Grant Nos. 96-02-17517, 96-15-96548, and 97-02-17003 is acknowledged. The authors thank I. Thompson and K. Jones for a careful reading of the manuscript and useful comments.

APPENDIX A: STANDARD HYPERSPHERICAL METHOD MATRIX ELEMENTS

To solve the three-body problem the following MEs should be calculated (in Jacobi system 3):

$$\langle V_{12}(\mathbf{X})\rangle\left\langle V_{23}\left(\mathbf{Y}-\frac{A_1}{A_1+A_2}\mathbf{X}\right)\right\rangle\left\langle V_{31}\left(\mathbf{Y}+\frac{A_2}{A_1+A_2}\mathbf{X}\right)\right\rangle. \tag{A1}$$

The main problem of ME calculations for the realistic binary (l-dependent, etc.) potentials is that any basis functions for more than two particles have definite relative angular momentum only for one pair of particles. So only $\langle V_{12}(\mathbf{X})\rangle$ could be calculated easily. In the HH method this problem is resolved by the Raynal-Revai coefficient formalism [34]. These coefficients expand HHs in one Jacobi system (number i) over HHs in the other Jacobi system (number j):

$$\mathcal{J}^{l_xl_y}_{KLS}(i)=\sum_{l_xl_y} R^{l_xl_y}_{\overline{l}_x\overline{l}_y}(j\to i;KL)\mathcal{J}^{\overline{l}_x\overline{l}_y}_{KLS}(j).$$

It allows to express MEs in any Jacobi system i via those in the system $k\neq i,j$, where the argument of potential V_{ij} is coordinate $\mathbf{X}$ (in such system only integration over $d\theta$ is numerical):

$$\begin{aligned}(\mathcal{J}^{l'_xl'_y}_{K'L'S'}(i)|V_{ij}|\mathcal{J}^{l_xl_y}_{KLS}(i))&\\ =\sum_{\overline{l}'_x\overline{l}'_y\overline{l}_x\overline{l}_y} R^{l'_xl'_y}_{\overline{l}'_x\overline{l}'_y}(k\to i;K'L')R^{l_xl_y}_{\overline{l}_x\overline{l}_y}(k\to i;KL)&\\ \times(\mathcal{J}^{\overline{l}'_x\overline{l}'_y}_{K'L'S'}(k)|V_{ij}|\mathcal{J}^{\overline{l}_x\overline{l}_y}_{KLS}(k)).&\end{aligned} \tag{A2}$$

Nuclear potentials are ordinary considered up to f waves, where they could be restricted by the experimental data. For higher partial waves the potentials are taken to be zero.

The Coulomb interaction is purely central and it is too time consuming to calculate its MEs for high K values using the procedure (A2) described above. The second and third MEs in Eq. (A1) of Coulomb potentials for a homogeneously charged sphere radius r_{0ij} are calculated using expansions over spherical functions:

$$V_{ij}^{(c)}(r_{ij})=\begin{cases}\dfrac{Z_1Z_2\alpha}{r_{ij}} & \text{for } r_{ij}>r_{0ij},\\ \dfrac{Z_1Z_2\alpha}{2r_{0ij}}\left(3-\dfrac{r_{ij}^2}{r_{0ij}^2}\right) & \text{for } r_{ij}\leqslant r_{0ij},\end{cases} \tag{A3}$$

$$V_{ij}^{(c)}(|\mathbf{Y}+C_{ij}\mathbf{X}|)=\sum_{l=l_{\min}\cdots l_{\max}}(C_{ij}/|C_{ij}|)^l \times[Y_l(\hat{X})\otimes Y_l(\hat{Y})]_{00}v_{ij}^{(l)}(X,Y).$$

The coefficients C_{ij} for the third Jacobi system are given in Eq. (A1):

$$v_{ij}^{(l)}(X,Y)=2\pi(-)^l\hat{l}\times\int_{-1}^{1}d\tau\,P_l(\tau)V_{ij}^{(c)}(\sqrt{C_{ij}^2X^2+Y^2+2C_{ij}XY\tau}). \tag{A4}$$

Integration in Eq. (A4) could be done analytically for $V_{ij}^{(c)}$ given by Eq. (A3):

$$(\mathcal{J}^{l_x'l_y'}_{K'L'S'S_x'}(i)|V_{ij}^{(c)}|\mathcal{J}^{l_xl_y}_{KLSS_x}(i))=\sum_{l=l_{\min}\cdots l_{\max}}\frac{(-)^{l_x+l_y'+l+L}}{4\pi}\frac{\hat{l}^2\hat{l}_x\hat{l}_y}{\hat{l}_y'}\times\begin{Bmatrix}l_y & l_x & L\\ l_x' & l_y' & l\end{Bmatrix}C^{l_x'0}_{l_y'0l0}C^{l_x0}_{l_y0l0}\delta_{L'L}\delta_{S'S}\times\int_0^{\pi/2}\psi^{l_x'l_y'}_{K'}(\theta)v_{ij}^{(l)}(X,Y)\psi^{l_xl_y}_{K}(\theta)\sin^2(\theta)\cos^2(\theta)d\theta.$$

Intermediate angular momenta l have very few allowed values, $l_{\min}=\max(|l_x'-l_x|,|l_y'-l_y|)$ and $l_{\max}=\min(l_x'+l_x,l_y'+l_y)$, making the numerical part of the calculations very compact.

APPENDIX B: ADDITIONAL MATRIX ELEMENTS FOR THE BINARY CHANNEL EQUATION

Using the hyperspherical decomposition (15) and (16) of the BC function, the ME used in Eqs. (17) and (18) can be written as

$$A_i(\rho)=\frac{2}{\phi_i(\rho)}\sum_K^{+}\sum_{\bar{\gamma}_i}\overline{\chi}^{l}_{K\bar{\gamma}_i}(\rho)\frac{d\overline{\chi}^{l}_{K\bar{\gamma}_i}(\rho)}{d\rho}, \tag{B1}$$

$$B_i(\rho)=\frac{1}{\phi_i(\rho)}\sum_K^{+}\sum_{\bar{\gamma}_i}\overline{\chi}^{l}_{K\bar{\gamma}_i}(\rho)\left[\frac{d^2}{d\rho^2}-\frac{\mathcal{L}(\mathcal{L}+1)}{\rho^2}-2M\{E_{3\text{sep}}+V_{K\bar{\gamma}_i,K\bar{\gamma}_i}(\rho)\}\right]\overline{\chi}^{l}_{K\bar{\gamma}_i}(\rho), \tag{B2}$$

$$C_{i'i}(\rho)=\frac{2M}{\phi_i(\rho)}\sum_{K'K}^{++}\sum_{\bar{\gamma}_{i'}\bar{\gamma}_i}V_{K'\bar{\gamma}_{i'},K\bar{\gamma}_i}(\rho)\overline{\chi}^{l'}_{K'\bar{\gamma}_{i'}}(\rho)\overline{\chi}^{l}_{K\bar{\gamma}_i}(\rho),$$

$$D_{K'\gamma'i}(\rho)=\frac{2M}{\phi_i(\rho)}\sum_K^{+}\sum_{\bar{\gamma}_i}V_{K\bar{\gamma}_i,K'\gamma'}(\rho)\overline{\chi}^{l}_{K\bar{\gamma}_i}(\rho),$$

$$E_{K\gamma,i'\bar{\gamma}_{i'}}(\rho)=2M\sum_{K'}^{+}V_{K\gamma,K'\bar{\gamma}_{i'}}(\rho)\overline{\chi}^{l'}_{K'\bar{\gamma}_{i'}}(\rho),$$

where

$$\sum_K^{-}\equiv\sum_{K=K^{(3)}_{\min}}^{K^{(3)}_{\max}},\qquad \sum_K^{+}\equiv\sum_{K=K^{(3)}_{\max}+2}^{K^{(2)}_{\max}},$$

$$\phi_i(\rho)=\sum_K^{+}\sum_{\bar{\gamma}_i}\{\overline{\chi}^{l}_{K\bar{\gamma}_i}(\rho)\}^2. \tag{B3}$$

We cannot improve the computation of the MEs $C_{i'i}$, $D_{K'\gamma'i}$, and $E_{K\gamma,i'\bar{\gamma}_{i'}}$ (if we are using noncentral potentials) in any other way than increasing $K^{(2)}_{\max}$. But we can improve the computation of $A_i(\rho)$, Eq. (B1), and $\phi_i(\rho)$, Eq. (B3), at large ρ using an exact form of $\mathcal{B}_i^{\text{ort}}$:

$$\mathcal{B}_i^{\text{ort}}(\mathbf{X},\mathbf{Y})=\mathcal{B}_i(\mathbf{X},\mathbf{Y})-\sum_K^{-}\sum_{\bar{\gamma}_i}\overline{\chi}^{l}_{K\bar{\gamma}_i}(\rho)\mathcal{J}_{K,\bar{\gamma}_i}(\Omega_5).$$

Then

$$\phi_i(\rho)=(\mathcal{B}_i|\mathcal{B}_i)-\sum_K^{-}\sum_{\bar{\gamma}_i}\{\overline{\chi}^{l}_{K\bar{\gamma}_i}(\rho)\}^2,$$

$$A_i(\rho)=\frac{4J^2}{\phi_i(\rho)}\left[\frac{\psi_{l_x j_x}\psi_{l_y}}{XY}\left|\frac{5\psi_{l_x j_x}\psi_{l_y}}{2XY}+\frac{\sin\theta}{C_x}\frac{\psi_{l_y}}{Y}\left(\frac{\psi_{l_x j_x}}{X}\right)'_X\right.\right.$$
$$\left.+\frac{\cos\theta}{C_y}\frac{\psi_{l_x j_x}}{X}\left(\frac{\psi_{l_y}}{Y}\right)'_Y\right]$$
$$-\frac{2}{\phi_i(\rho)}\sum_K^{-}\sum_{\gamma_i}\overrightarrow{\chi}^{l}_{K\bar{\gamma}_i}(\rho)\frac{d\overrightarrow{\chi}^{l}_{K\bar{\gamma}_i}(\rho)}{d\rho}. \quad \text{(B4)}$$

C_x and C_y are defined in Eqs. (1) and (2), $J=(C_xC_y)^{-3}$. For $\rho\to 0$ this method is less reliable than that given by Eqs. (B1) and (B3), so both methods were combined in the calculations.

The most complicated is ME (B2), which can be written in symbolic form as

$$B_i(\rho)=-\frac{2M}{\phi_i(\rho)}(\mathcal{B}_i^{\rm ort}|\hat{H}-E|\mathcal{B}_i^{\rm ort}),$$

where $\mathcal{B}_i^{\rm ort}$ is *asymptotically* an eigenfuncton of Hamiltonian, such that $B_i(\rho)\overset{\rho\to\infty}{\to}0$. However, the ME of the kinetic energy, $\phi_i(\rho)^{-1}(\mathcal{B}_i^{\rm ort}|\hat{T}|\mathcal{B}_i^{\rm ort})$, is decreasing slowly. Such a behavior is in principle compensated by the MEs of potentials entering into the Hamiltonian. In practice the hyperspherical MEs of potentials decrease quite rapidly with ρ (for given $K^{(2)}_{\rm max}$), so the $K^{(2)}_{\rm max}$ value, which we have to use to achieve correct behavior for $B_i(\rho)$, can be unreasonably large. Decomposing the operator $\hat{T}$ in $\hat{T}_x+\hat{T}_y$ it is possible to find that for

$$E_x>E_y \quad \text{(B5)}$$

the long-range behavior of $B_i(\rho)$ is connected to the ME of kinetic energy ($\hat{T}_x$), and otherwise with ($\hat{T}_y$) [E_x and E_y are the binding energies of the subsystems (11) and (13)]. It allows us to subtract the kinetic energy ME analytically for the physical situation of interest, when the binary system is weakly bound with respect to the third particle. If we cannot perform subtraction (binary subsystem is deeply bound), $f(\rho)$ would not achieve the correct asymptotic behavior (in the realistic calculation). However, we can exploit the high flexibility of the BC function even in that case. Using the property of the function $\mathcal{B}_i$,

$$(\hat{H}-E)\mathcal{B}_i=(\hat{V}_{23}+\hat{V}_{31}-V_y)\mathcal{B}_i,$$

where V_y is the potential which was used to construct the function $\psi_{l_y}(Y)$, one can obtain another expression for $B_i(\rho)$:

$$B_i(\rho)=\frac{2M}{\phi_i(\rho)}\left\{(\mathcal{B}_i|V_y|\mathcal{B}_i)-2\sum_K^{-}\sum_{\gamma_i}(\mathcal{B}_iV_y|\mathcal{J}_{K,\alpha l_y})\overrightarrow{\chi}^{l}_{K\bar{\gamma}_i}(\rho)\right.$$
$$-\sum_{K'K}^{--}\sum_{\gamma_{i'}\gamma_i}(\mathcal{J}_{K'\bar{\gamma}_{i'}}|\hat{V}_{12}|\mathcal{J}_{K\bar{\gamma}_i})\overrightarrow{\chi}^{l'}_{K\bar{\gamma}_{i'}}(\rho)\overrightarrow{\chi}^{l}_{K\bar{\gamma}_i}(\rho)$$
$$-\sum_{K'K}^{++}\sum_{\gamma_{i'}\gamma_i}(\mathcal{J}_{K'\bar{\gamma}_{i'}}|\hat{V}_{23}+\hat{V}_{31}|\mathcal{J}_{K\bar{\gamma}_i})\overrightarrow{\chi}^{l'}_{K\bar{\gamma}_{i'}}(\rho)\overrightarrow{\chi}^{l}_{K\bar{\gamma}_i}(\rho)$$
$$+\sum_K^{-}\sum_{\gamma_i}\overrightarrow{\chi}^{l}_{K\bar{\gamma}_i}(\rho)\left[\frac{d^2}{2Md\rho^2}-\frac{\mathcal{L}(\mathcal{L}+1)}{2M\rho^2}-E_{\rm 3sep}\right]$$
$$\left.\times\overrightarrow{\chi}^{l}_{K\bar{\gamma}_i}(\rho)\right\}. \quad \text{(B6)}$$

The ME obtained with Eq. (B6) has the wrong behavior at $\rho<5-8$ fm (for numerical reasons). If $K^{(2)}_{\rm max}$ is high enough, then Eq. (B6) overlaps with Eq. (B2) in a wide range, so they can be easily combined. For high $K^{(2)}_{\rm max}$ [$K^{(2)}_{\rm max}=40-70$ for Eqs. (B2) and (B6) or $K^{(2)}_{\rm max}=20-40$ for Eqs. (B1) and (B4)] different methods of ME calculation give the same result up to 20–25 fm, supplying us a good check as to how far we can go in ρ values without loss of calculation consistency.

[1] N. B. Shul'gina, B. V. Danilin, V. D. Efros, J. M. Bang, J. S. Vaagen, and M. V. Zhukov, Nucl. Phys. **A597**, 197 (1996).

[2] L. V. Grigorenko, B. V. Danilin, V. D. Efros, N. B. Shul'gina, and M. V. Zhukov, Phys. Rev. C **57**, R2099 (1998).

[3] F. C. Barker, Nucl. Phys. **A588**, 693 (1995).

[4] M. V. Zhukov, B. V. Danilin, D. V. Fedorov, J. M. Bang, I. J. Thompson, and J. S. Vaagen, Phys. Rep. **231**, 151 (1993).

[5] P. G. Hansen, A. S. Jensen, and B. Jonson, Annu. Rev. Nucl. Part. Sci. **45**, 591 (1995).

[6] I. Tanihata, J. Phys. G **22**, 157 (1996).

[7] B. V. Danilin, M. V. Zhukov, A. A. Korsheninnikov, and L. V. Chulkov, Yad. Fiz. **53**, 71 (1991) [Sov. J. Nucl. Phys. **53**, 45 (1991)].

[8] A. Kievsky, M. Viviani, and S. Rosati, Nucl. Phys. **A551**, 241 (1993).

[9] B. N. Zakhar'ev, V. V. Pustovalov, and V. D. Efros, Yad. Fiz. **8**, 406 (1968) [Sov. J. Nucl. Phys. **8**, 234 (1969)].

[10] M. V. Zhukov and V. D. Efros, Yad. Fiz. **14**, 577 (1971) [Sov. J. Nucl. Phys. **14**, 577 (1972)].

[11] V. D. Efros and M. V. Zhukov, Phys. Lett. **37B**, 18 (1971).

[12] A. N. Vostrikov and M. V. Zhukov, Yad. Fiz. **34**, 344 (1981) [Sov. J. Nucl. Phys. **34**, 195 (1981)].

[13] H. Feshbach, Ann. Phys. (N.Y.) **5**, 375 (1958); **19**, 287 (1962).

[14] K. Wildermuth and Y. Tang, *A Unified Theory of the Nucleus* (Vieweg, Braunschweig, 1977).

[15] D. R. Lehman and W. C. Parke, Phys. Rev. C **29**, 2319 (1984); A. Eskandarian, D. R. Lehman, and W. C. Parke, *ibid.* **39**, 1685 (1989).

[16] E. Garrido, D. V. Fedorov, and A. S. Jensen, Nucl. Phys. **A650**, 247 (1999).

[17] D. R. Tilley, H. R. Weller, and H. H. Hasan, Nucl. Phys. **A474**, 1 (1987).
[18] D. R. Tilley, H. R. Weller, and G. M. Hale, Nucl. Phys. **A541**, 1 (1992).
[19] N. W. Schellingerhout, L. P. Kok, S. A. Coon, and R. M. Adam, Phys. Rev. C **48**, 2714 (1993); **52**, 439 (1995).
[20] S. Sack, L. C. Biedenharn, and G. Breit, Phys. Rev. **93**, 321 (1954).
[21] B. V. Danilin, M. V. Zhukov, A. A. Korsheninnikov, V. D. Efros, and L. V. Chulkov, Yad. Fiz. **48**, 1208 (1988) [Sov. J. Nucl. Phys. **48**, 766 (1988)].
[22] F. Ajzenberg-Selove, Nucl. Phys. **A490**, 1 (1988).
[23] H. M. Xu, C. A. Gagliardi, R. E. Tribble, A. M. Mukhamedzhanov, and N. K. Timofeyuk, Phys. Rev. Lett. **73**, 2027 (1994).
[24] N. K. Timofeyuk, D. Baye, and P. Descouvemont, Nucl. Phys. **A620**, 29 (1997).
[25] P. Descouvemont and D. Baye, Nucl. Phys. **A487**, 420 (1988).
[26] K. Varga, Y. Suzuki, and I. Tanihata, Phys. Rev. C **52**, 3013 (1995).
[27] A. Csóto, Phys. Lett. B **315**, 24 (1993).
[28] H. Stöwe and W. Zahn, Nucl. Phys. **A289**, 317 (1977).
[29] H. D. Knox and R. O. Lane, Nucl. Phys. **A359**, 131 (1981).
[30] L. V. Grigorenko, N. B. Shul'gina, and M. V. Zhukov, Nucl. Phys. **A607**, 277 (1996); **A614**, 567(E) (1997).
[31] V. Z. Goldberg, G. V. Rogachev, M. S. Golovkov, V. I. Dukhanov, I. N. Serikov, and V. A. Timofeev, Pis'ma Zh. Éksp. Teor. Fiz. **67**, 959 (1998) [JETP Lett. **67**, 1013 (1998)].
[32] A. Mengoni, T. Motobayashi, and T. Otsuka, nucl-th/9809052.
[33] M. H. Smedberg *et al.*, Phys. Lett. B **452**, 1 (1999).
[34] J. Raynal and J. Revai, Nuovo Cimento **68**, 612 (1970).